

Investigation of formation of precipitates and solidification temperatures of ferritic stainless steels using differential scanning calorimetry and Thermo-Calc simulation

David Sasu Konadu^{1,2}, Pieter Georg Hendrik Pistorius¹

1. Department of Materials Science and Metallurgical Engineering, University of Pretoria, Pretoria 0002, South Africa

2. Department of Materials Science and Engineering, University of Ghana, P. O. Box LG 77, Legon-Accra, Ghana

Corresponding author

D. S. Konadu, email address: dskonadu@ug.edu.gh, Mobile No.: 00233-507230358

Abstract

The phase transformations in unstabilized and stabilized ferritic stainless steels during solidification were studied using Thermo-Calc and differential scanning calorimetry (DSC). The solidus and liquidus temperatures of the Thermo-Calc simulations were compared to the liquidus and solidus temperatures measured with DSC. Thermo-Calc software revealed the precipitates of the ferritic stainless steels to be MnS, TiN, Ti₄C₂S₂, NbC, and Ti(C,N). Given the low volume fraction of precipitates, DSC could not be used to reveal the onset of precipitation. There was reasonable correlation between the difference between the liquidus and the solidus temperature, as calculated using Thermo-Calc and as measured using DSC. Generally, a higher niobium content resulted in a higher solidification temperature range.

Keywords: Thermo-Calc; differential scanning calorimetry (DSC); ferritic stainless steel; solidification temperature range; solidus and liquidus.

1. Introduction

Ferritic stainless steels are iron-chromium alloys containing about 12 – 30 wt% Cr with a carbon content of 0.25% maximum. Rapid grain growth occurs for ferritic stainless steels that are held above 1100°C in the δ -ferrite region. The grain boundaries become enriched with impurities and the ductile-to-brittle transition temperature (DBTT) increases [1]. On cooling from high temperatures, ferritic stainless steels often suffer from precipitation of carbides and nitrides in the matrix. These precipitates are distributed randomly or aligned along grain boundaries [2]. In general, ferritic stainless steels have low solubility for carbon at ambient temperatures. Chromium-rich carbides precipitate as $M_{23}C_6$ and if the carbon content is high, as M_7C_3 . In the presence of Mo, M_6C forms. These carbides have a chromium content typically in the range of 42 to 65%, resulting in chromium depleted zones adjacent to the grain boundary precipitates. If the depletion is below 12 wt%, intergranular corrosion attack progresses along the chromium depleted grain boundaries since the corrosion resistance is significantly reduced. In corrosive conditions, the grain boundaries are preferentially attacked; such localised attack may lead to grain dropping. This is known as sensitization. These can be prevented by reducing either the carbon and nitrogen amounts below certain levels or using titanium, niobium or tantalum as stabilizers [1, 3, 4]. Titanium and niobium have a high affinity for carbon and nitrogen. As such, they are used as stabilizers to arrest carbon and nitrogen in stainless steels by forming stable carbides, nitrides or carbonitrides to prevent sensitization [5-6]. Ti additions to ferritic stainless steel improves pitting resistance, pins the grain boundaries of the heat affected zones, and results in fine grained equiaxed structure. Excess Ti strengthens the ferritic stainless steels by solid solution strengthening. Ti additions may result in a poor surface finish of the steel sheet. Nb addition in ferritic stainless steels forms small spherical precipitates. Ferritic stainless steels with Nb additions do not show poor surface finish. However, ferritic

stainless steels with Nb may suffer in low ductility in the welded joint [6]. Nb is a high temperature solid solution strengthener in ferritic stainless steels [7–9].

Differential scanning calorimetry (DSC) can be used to study the phase transformations that occur upon heating and cooling of various alloys, including ferritic stainless steels [10-11]. Two widely used DSC systems are heat flux DSC and power-compensated DSC. With the heat flux DSC, also called quantitative differential thermal analysis, the temperature difference between the sample and an inert reference body is measured directly. The temperature difference is converted to a heat flow. In the power compensated DSC, two separate chambers contain the sample and the reference, and each chamber has its individual heating element for temperature control. An increase in power to heat the sample occurs during an endothermic event and a reduction in power to cool the sample occurs in an exothermic event. The compensation for heat release or gain of the sample is measured by the difference in the amount of power between the sample and the reference [11]. The electrical power needed for temperature equalization is plotted against temperature. Peaks may be characterized by calculating the energy per unit mass [10].

Recent work on susceptibility to solidification cracking of ferritic stainless steels using the testing methods of self-restrained Houldcroft and Modified Vareststraint Transvareststraint, the solidification temperature range was not measured. Only Thermo-Calc simulation results were presented [12-13]. It was therefore necessary to measure the solidification temperature range as the solidification temperature range is also the brittle temperature range which can be approximated by the difference between the liquidus and solidus temperatures of a material [3, 14]. In this paper, a comparison of the solidification temperature range of nine unstabilized and stabilized ferritic stainless steels, as determined using Thermo-Calc simulations and as measured using power compensated differential scanning calorimetry is presented.

2. Experimental method

The chemical composition of the all as cast unstabilized and stabilized ferritic stainless steels is shown in table 1. Two unstabilized steels, one steel stabilized only by Ti, one steel stabilized by only Nb and five dual (Ti +Nb) stabilized steels were included in the experimental matrix. Thermo-Calc version 2015b (TCFE6 database) software was used to identify the phases (liquid or BCC) for all the alloys and the precipitates present at a range of temperatures. This was done through thermodynamic equilibrium and phase diagram calculations using the full chemical compositions as shown in table 1. The same calculations yielded the mole fraction of all phases at every temperature, for the alloys showed in table 1.

For the DSC experiment, the samples were machined to approximate dimensions of 5 mm diameter and 2 – 3 mm height. With the exception of alloy H:0.1Ti;0.4Nb which was not used for this experiment because it was not available at the time of the DSC experiment, sample A had a mass of about 293 mg. The other samples had a mass between 393 and 395 mg. Power compensated DSC thermal analysis was done with a Netzsch STA409 instrument. The DSC experiments were performed in a static atmosphere of 99.99% purity argon at a pressure of about 1000 mbar inside a graphite furnace chamber, to prevent contamination and minimize oxidation of the sample. An alumina crucible was used as the reference. A heating and cooling rate of 5 K/min was used. The furnace was heated to 1500°C. The maximum sample temperature (about 1500°C) was very close to the liquidus temperature (estimated using Thermo-Calc simulations at 1490 to 1500°C [table 2]). There was a holding time of 5 minutes before cooling started to ensure that the sample was fully melted. From the work by Ganesh et al. [15] and Petrovic et al. [16], it is likely that equilibrium conditions were reached.

3. Results

3.1 Results of the Thermo-Calc simulation

Figures 1 - 3 show the results of the Thermo-Calc simulations for the A:0Ti;0Nb, C:0.7Ti and E:0.4Ti;0.6Nb alloys respectively. Table 2 shows the phases in equilibrium with liquid metal, solidus, liquidus and the solidification temperature range of the alloys used for this project. It can be seen that the addition of Nb to the unstabilized alloy decreased the solidus temperature from 1433 to 1387°C. The addition of Ti increased the solidus temperature to 1470°C. The dual stabilized steels had an estimated solidus temperature similar to that of the steels that contained only Ti. From table 2, the possible precipitates that will be expected within the liquidus and solidus temperatures for all the ferritic stainless steels are MnS, TiN, Ti₄C₂S₂, NbC, and Ti(C,N). It can also be seen that the predicted fractions of precipitates were very low (figures 1-3), never exceeding a mole fraction of 0.01.

The solidus and liquidus temperatures were clearly visible from the Thermo-calc simulation results (figures 1-3). The interval between the two temperatures, the solidification temperature range (ΔT), revealed that there was a decrease in ΔT when Ti (C:0.7Ti) was added to the unstabilized steel (A:0Ti;0Nb). With the addition of Nb, the ΔT increased to the highest value (table 2) [17]. It is interesting to note that, the highest Nb content in the dual stabilized steel (F:0.4Ti;0.9Nb) revealed the second highest value of ΔT , presumably due to the titanium content. From figure 1b, the formation of MnS and AlN precipitates only formed below the solidus temperature. The addition of Ti resulted in the formation of TiN and Ti₄C₂S₂ between the liquidus and the solidus temperature (figure 2b). The simultaneous addition of Ti and Nb resulted in the formation of TiN and Ti[C,N], precipitates in the mushy zone (figure 3b). This agrees with Park [18].

Table 1. Actual chemical composition of type AISI 430, 436, 439, 441 and 444 ferritic stainless steels.

Element	Composition (mass %)								
	A:0Ti;0Nb	B:0Ti;0Nb	C:0.7Ti	D:0.6Nb	E:0.4Ti;0.6Nb	F:0.4Ti;0.9Nb	G:0.1Ti;0.4Nb	H:0.1Ti;0.4Nb	I:0.1Ti;0.5Nb;2Mo
C	0.006	0.046	0.006	0.012	0.017	0.011	0.013	0.011	0.015
Si	0.600	0.450	0.610	0.420	0.400	0.440	0.510	0.490	0.530
Mn	0.510	0.360	0.500	0.330	0.370	0.370	0.440	0.430	0.440
P	0.019	0.020	0.018	0.024	0.022	0.025	0.024	0.025	0.033
S	0.008	0.002	0.007	0.007	0.001	0.004	0.013	0.002	0.003
N	0.069	0.055	0.069	0.070	0.069	0.067	0.013	0.015	0.018
Cr	18.030	16.070	17.940	18.810	18.120	18.170	17.660	17.500	18.100
Nb	0.010	0.001	0.003	0.580	0.620	0.920	0.422	0.396	0.535
Ti	0.001	0.001	0.680	0.030	0.410	0.360	0.146	0.112	0.096
Ni	0.230	0.270	0.240	0.230	0.350	0.370	0.150	0.150	0.160
V	0.007	0.100	0.040	0.050	0.110	0.110	0.130	0.120	0.130
Cu	0.010	0.070	0.020	0.060	0.060	0.070	0.050	0.070	0.080
Al	0.200	0.009	0.180	0.030	0.020	0.020	0.012	0.010	0.014
Mo	0.020	0.005	0.020	0.020	0.020	0.020	0.014	0.011	2.000
Fe	Bal	Bal	Bal	Bal	Bal	Bal	Bal	Bal	Bal

Table 2. Results of Thermo-Calc modelling of the experimental matrix showing nominal Ti and Nb content.

Steel ID	Grade	Ti	Nb	Liquidus temperature (T_L) (°C)	Solid state phases in equilibrium with liquid metal	Solidus temperature (T_S) (°C)	$T_L - T_S$ (°C)
A:0Ti;0Nb	430	0.0	0.0	1500	Ferrite and MnS	1433	67
B:0Ti;0Nb	430	0.0	0.0	1500	Ferrite and MnS	1411	89
C:0.7Ti	439	0.7	0.0	1500	Ferrite, TiN, and $Ti_4C_2S_2$	1448	52
D:0.6Nb	436	0.0	0.6	1497	Ferrite, NbC, and MnS	1387	110
E:0.4Ti;0.6Nb	441	0.4	0.6	1500	Ferrite, Ti(C,N), and $Ti_4C_2S_2$	1448	52
F:0.4Ti;0.9Nb	441	0.4	0.9	1500	Ferrite, TiN, and $Ti_4C_2S_2$	1433	67
G:0.1Ti;0.4Nb	441	0.1	0.4	1500	Ferrite, Ti(C,N), and $Ti_4C_2S_2$	1470	30
H:0.1Ti;0.4Nb	441	0.1	0.4	1500	Ferrite, Ti(C,N), and $Ti_4C_2S_2$	1464	36
I:0.1Ti;0.5Nb;2Mo	444	0.1	0.5	1490	Ferrite, Ti(C,N), and $Ti_4C_2S_2$	1450	40

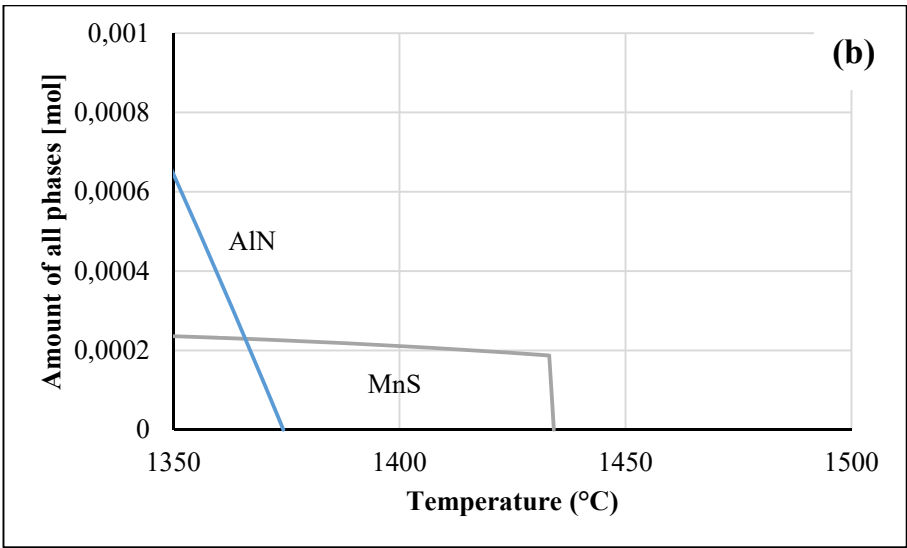
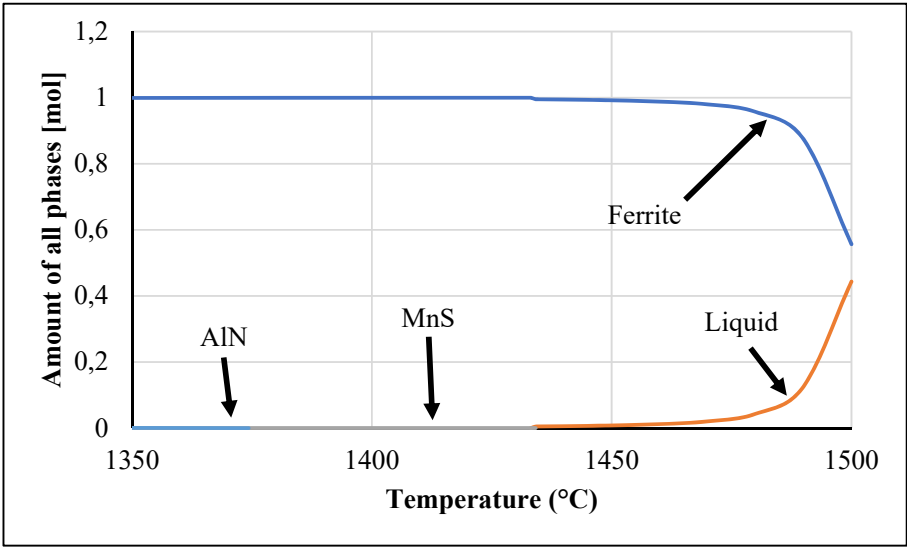


Figure 1. a) The possible precipitates from Thermo-Calc between 1350°C and 1500°C for sample A:0Ti;0Nb, and b) the molar fraction precipitate.

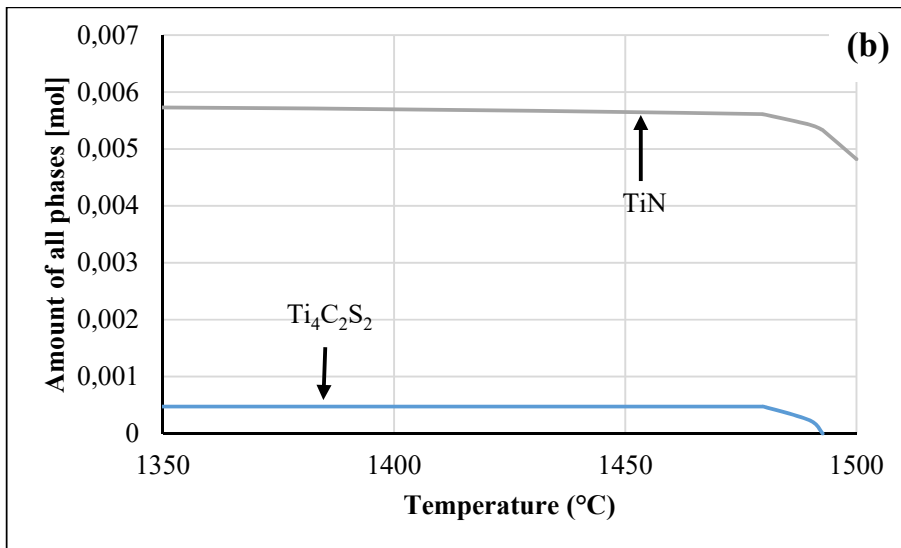
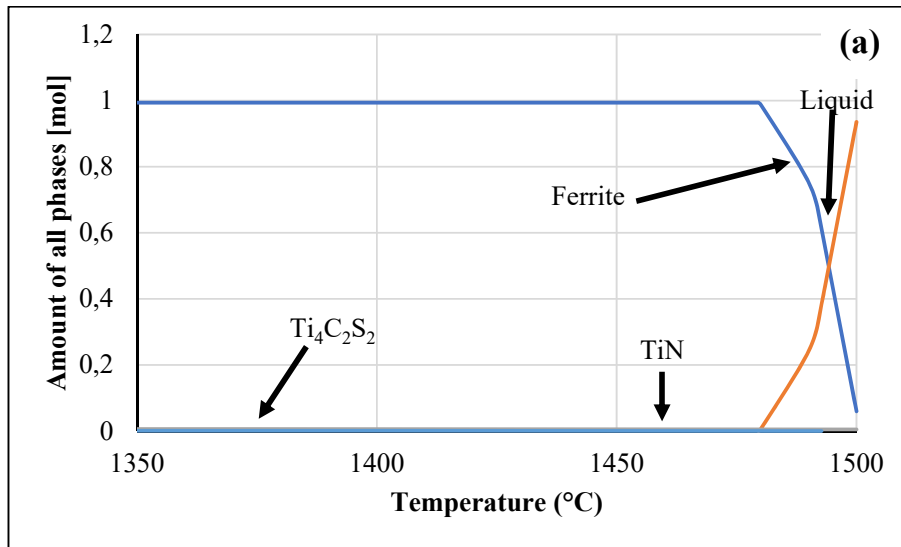


Figure 2. a) The possible precipitates from Thermo-Calc between 1350°C and 1500°C for sample C:0.7Ti, and b) the molar fraction precipitate.

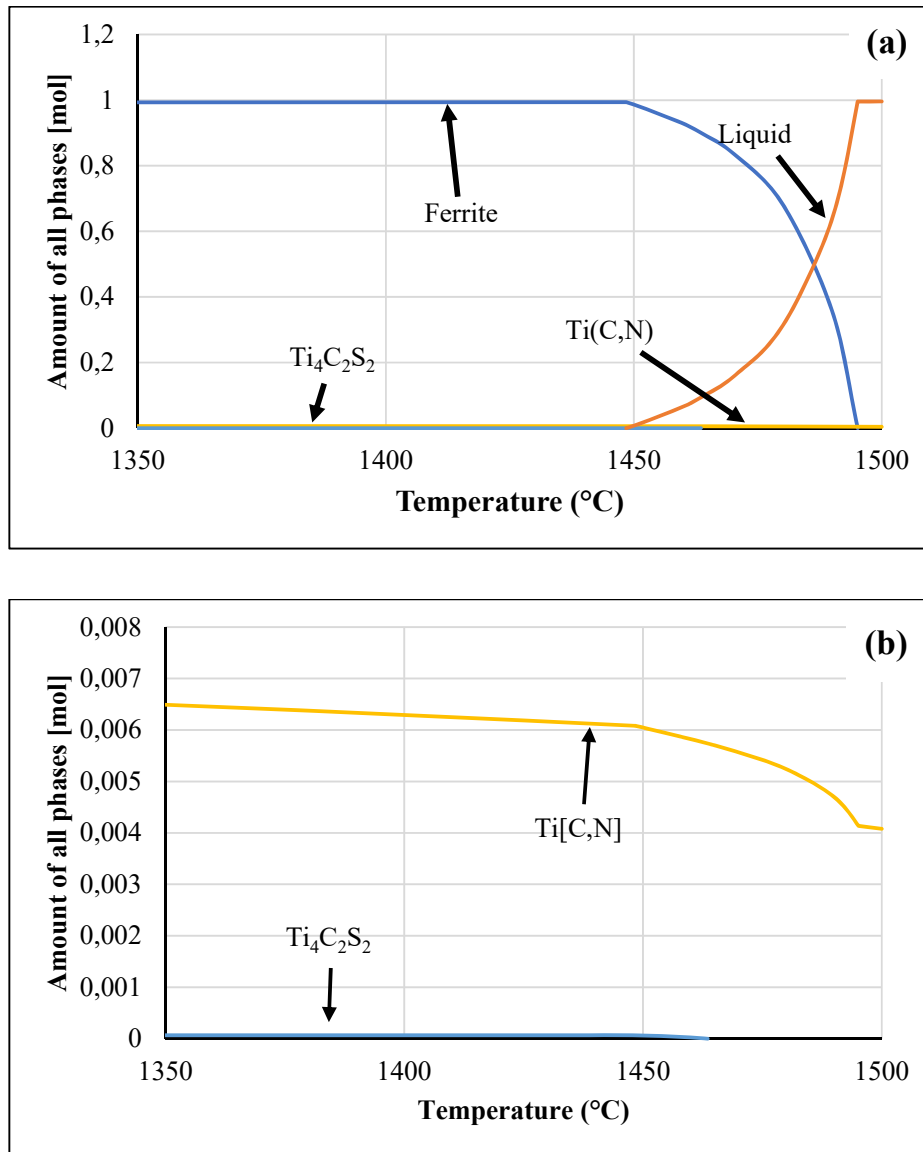


Figure 3. a) The possible precipitates from Thermo-Calc between 1350°C and 1500°C for sample E:0.4Ti;0.6Nb, and b) the molar fraction precipitate.

3.2 Results of the DSC measurements

A typical DSC thermogram recorded during slow heating to the liquidus temperature followed by slow cooling to room temperature of the sample E:0.4Ti;0.6Nb is presented in figure 4. The DSC melting thermogram was characterized by one endothermic peak by heating from 500°C till melting and the cooling curve by one exothermic peak. It could be seen that there was no change in the curves till when solidification started. Figure 4 was difficult to use to estimate

the solidus and liquidus temperatures. The high temperature behavior was replotted using the data to give the exploded view (figure 5). Not all the parameters (solidus and liquidus temperatures) could be determined (table 3), probably due to the fact that the liquidus temperature was very close to the maximum temperature that the DSC apparatus could reach (that is, 1500°C). It could also be that on heating, the indication associated with the liquidus temperature was generally poorly visible. Figures 6 and 7 show the superimposition of all the alloys during the heating and cooling curves respectively. It can be seen that there is not much differences between both curves. This shows the similar behavior of all the alloys. The exploded plot (figure 7) showed the different start of solidification with the solidification finish nearly coinciding.

All the DSC thermograms for the alloys followed similar behavior by showing straight lines from the start of melting to completion and the on-cooling curves followed similar behavior. DSC could therefore not be used to detect the formation of precipitates on cooling. This was consistent with the predicted low fraction of precipitates as noted earlier (also refer to figure 1). Table 3 shows the solidus, liquidus and the solidification temperature range for the alloys used in the DSC experiment for the on-heating and on-cooling cycles. The solidification temperature range values of the unstabilized steel A:0Ti;0Nb could not be estimated. The highest solidification temperature range was F:0.4Ti;0.9Nb (50°C). This was followed by E:0.4Ti;0.6Nb (39°C), both C:0.7Ti (32°C) and I:0.1Ti;0.5Nb;2Mo (32°C), D:0.6Nb (27°C) and G:0.1Ti;0.4Nb (16°C) (table 3).

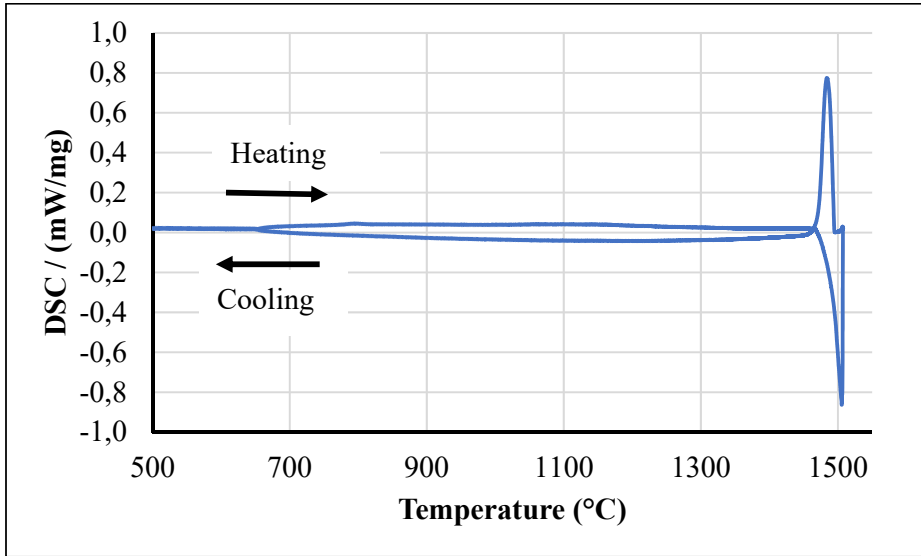


Figure 4. DSC thermogram for the sample E:0.4Ti;0.6Nb during heating and cooling.

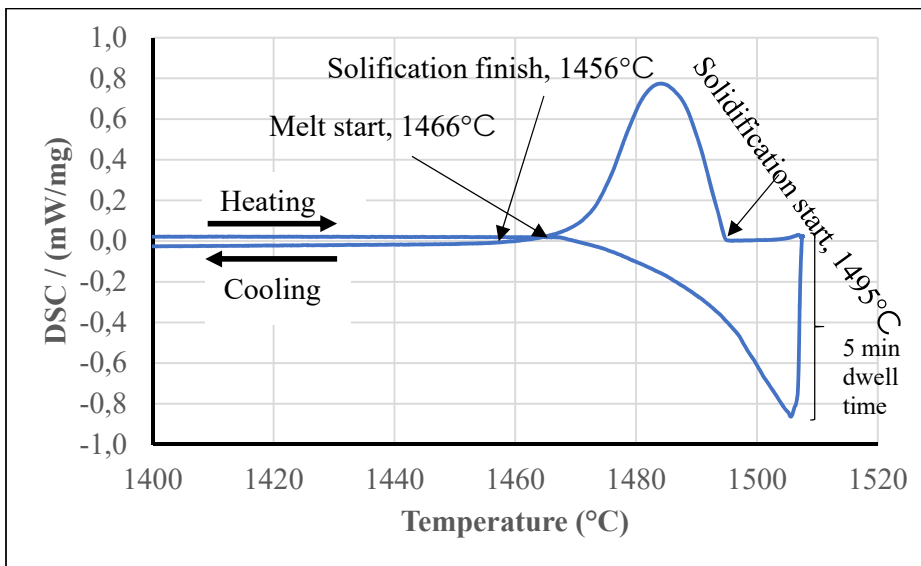


Figure 5. Expanded thermogram for alloy E:0.4Ti;0.6Nb showing the solidus and liquidus temperatures.

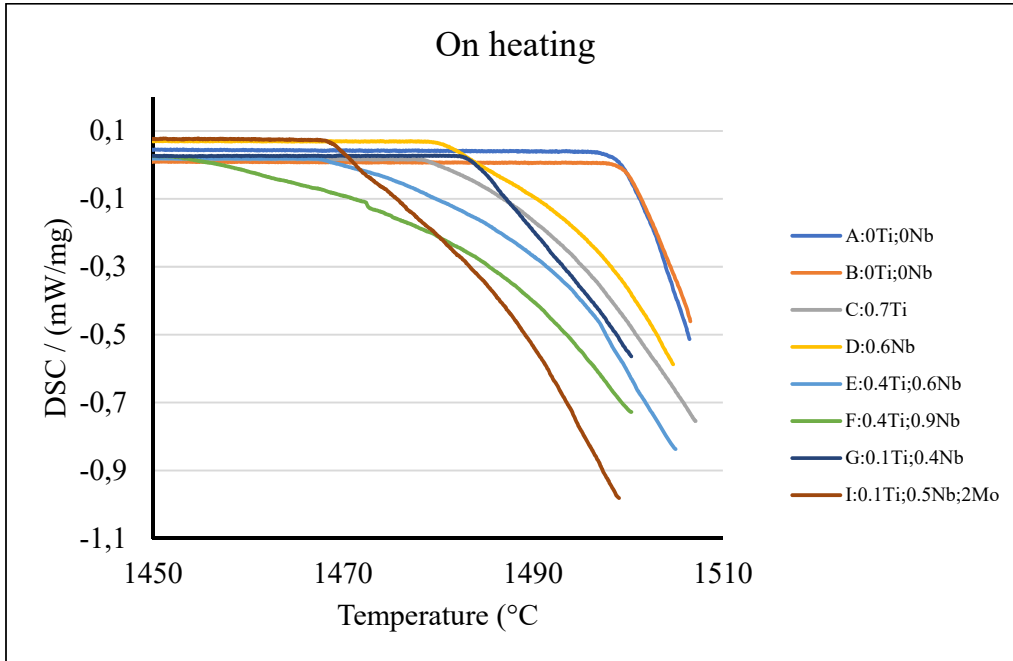


Figure 6. The superimposition of the heating curves of all the alloys.

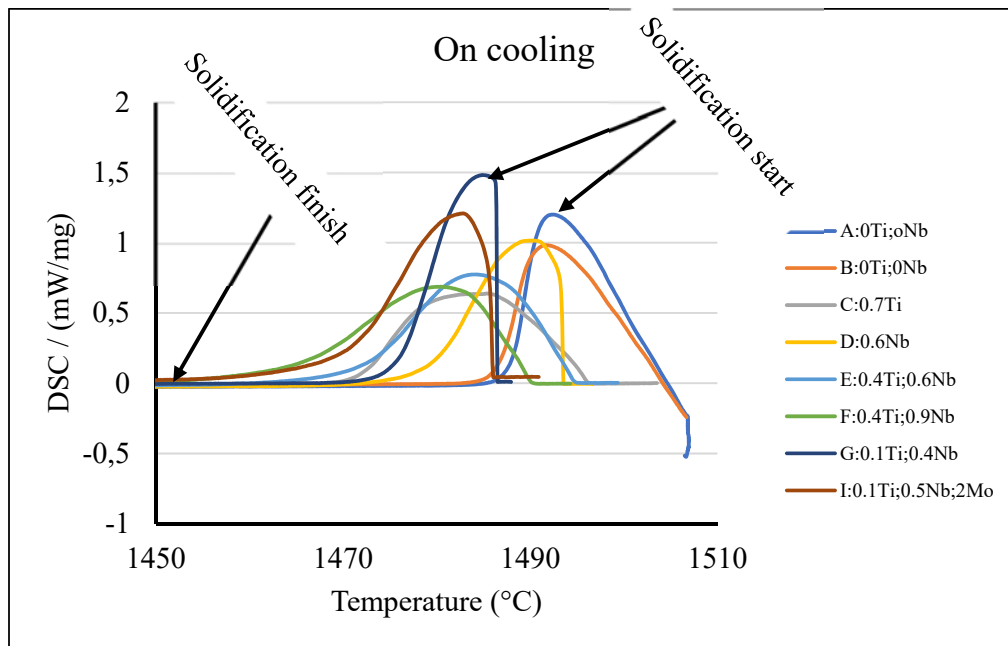


Figure 7. The superimposition of the cooling curves of all the alloys.

Table 3. DSC measurement (on cooling) results of the solidus and liquidus temperatures of the tested samples.

Sample ID	On heating			On cooling		
	Liquidus temperature (°C)	Solidus temperature (°C)	Solidification range (°C)	Liquidus temperature (°C)	Solidus temperature (°C)	Solidification range (°C)
A:0Ti;0Nb	--	1497	--	--	1483	--
B:0Ti;0Nb	--	1498	--	--	1482	--
C:0.7Ti	--	1478	--	1497	1465	32
D:0.6Nb	--	1480	--	1494	1467	27
E:0.4Ti;0.6Nb	--	1466	--	1495	1456	39
F:0.4Ti;0.9Nb	1505	1452	53	1490	1440	50
G:0.1Ti;0.4Nb	--	1482	--	1486	1470	16
I:0.1Ti;0.5Nb;2Mo	--	1466	--	1486	1454	32

4. Discussion

The addition of Nb to the unstabilized alloy decreased the solidus temperature. It has been reported that Nb forms a eutectic with Fe at 18.6% Nb with the melting point at 1373°C. The calculated solidus temperature of Alloy C (0.6%Nb, but not containing titanium) of 1387°C was therefore close to the eutectic temperature in the δ -ferrite – ϵ part of the Fe-Nb phase diagram [5, 14]. The precipitates MnS, TiN, Ti₄C₂S₂, NbC, and Ti(C,N) observed in the Thermo-Calc simulation have been experimentally observed [6, 15]. The addition of Nb to the unstabilized and the highest Nb content in the dual stabilized steel (F:0.4Ti;0.9Nb) revealed the second highest value of ΔT . This confirms the role of Nb in forming phases with a low melting point [5]. Shan et al. [17] reported that with Ti or Nb content increasing in ferritic stainless steels, the solidus temperature is reduced more, for the same increase in Ti or Nb, than the liquidus temperature using Thermo-Calc simulations. It was also stated that Nb contributed more than Ti in the solidification temperature range for the ferritic stainless steels [17]. The current results confirmed this behavior.

The DSC melting thermogram was characterized by one endothermic peak by heating till melting and the cooling curve by one exothermic peak. These peaks represents the melting of the δ -ferrite phase and solidification to δ -ferrite [21]. The solidification temperature range (BTR) during the cooling of the metal is approximated by the difference between the liquidus and solidus temperatures of a material [3, 19]. Tripathy et al [18] used the beginning of solidification of an austenitic stainless steel during cooling of a DSC experiment as the liquidus temperature of the alloy. Based on these statements, the cooling curve was used to estimate the liquidus and solidus temperatures of the alloys which corresponded to solidification start and finish respectively (figures 5 & 7). The cooling curve can be used to explain the mechanism of solidification of the ferritic stainless steels which represents the phase changes occurring in the alloy when it is solidifying/cooling [3, 12, 18]. Consider, for example, the DSC curves for all

the alloys in figure 7. During heating, the onset of melting and the completion of melting could not be observed. Presumably, complete melting occurred during the isothermal period at 1500°C. On cooling, the liquidus and the solidus temperature could be discerned from the exothermic peak (figure 5 & table 3). After the solidification, there was no phase change till room temperature. The highest solidification temperature range for the DSC experiment was F:0.4Ti;0.9Nb (50°C). This was contrary to Thermo-Calc results, which showed alloy D:0.6Nb as having the highest solidification temperature range (table 2). This could be attributed to the high Nb content in the alloy.

The solidification mechanism of all the ferritic stainless steels of above 16 wt% Cr showed a solidification temperature range during melting from on-heating and cooled through δ and α ferrite phases to room temperature without passing through austenite phase field. The amount of Cr, a ferrite former, was able to enlarge the ferrite phase field at the expense of the austenite phase region [1]. The effect of Ti and Nb was not observed on the solid phase (δ ferrite) in equilibrium with the liquid during solidification as the DSC spectra showed the same phase changes of δ and α ferrite during the on-heating and on-cooling cycles. A plot of the measured DSC solidus temperature values against the Nb content (neglecting the Ti content) showed a decreasing with increasing Nb content (figure 6). The decrease in solidus temperature with increasing Nb content was consistent with previously published Thermo-Calc simulations [17].

Comparing the on-cooling with the Thermo-Calc values (table 2), it can be seen that there were differences in values and this could be due to the discrepancy between the equilibrium conditions assumed for the Thermo-Calc simulation and the actual rate of temperature change (5°C/min). Petrovič et al. [16] reported that different scan rates produced non-identical liquidus temperatures for the same austenitic stainless steel. This was evident as the lowest liquidus temperature of 1442.9°C was measured at the fastest cooling rate and the

slower cooling rate produced the highest liquidus temperature of 1454.7°C. Generally, the liquidus temperature values of the DSC experiment were between 1486°C and 1497°C and that of the Thermo-Calc values were around 1500°C on average (figure 6). The solidus temperature values of the on-cooling DSC experiment were similar compared to that of the Thermo-Calc values, though some differences were found of same alloys (table 2). It has been shown that selected empirical equations for the liquidus and solidus temperatures were often not particularly accurate, though some predictions correlated well. Reasons for the differences between estimated and actual liquidus and solidus temperatures were given as the equipment arrangement, sample mass and sensitivity of sensors [22]. Also, the solidification temperature range was high for Thermo-Calc simulation compared to DSC experiment (tables 2 and 3). This might be due to the scan rate which has been found to give changes in such values [16].

The relationship between the DSC liquidus and solidus temperatures and that of the Thermo-Calc simulations is shown in figure 8. It could be seen that the DSC liquidus temperature values were either close to 1500°C or to the Thermo-Calc values except one (figure 8). With the solidus temperature values, the values were scattered (figure 8). Three of the solidus values were seen to be separated from the ideal line. These solidus values corresponded to the alloys A:0Ti;0Nb, B:0.7Ti and C:0.6Nb. At zero Nb, the solidification temperature range was above 30°C. This decreased to 16°C and then increased with increasing Nb content (figure 8). This reveals the harmful effect of Nb as it forms low melting eutectics to increase the solidification temperature range, which eventually increases the susceptibility to solidification cracking of ferritic stainless steels. For the steels that contained Nb, the estimated difference between the liquidus and the solidus temperature as a function of Nb content increases quite strongly with Nb content (figure 9). The results for the Thermo-Calc simulation and for the DSC for the solidification range differed by about 15°C. From the limited amount of data available, it seems that an increase in the Nb content of 1% results in an increase in the

solidification range around 67 to 69°C. Although the results for the Thermo-Calc estimate and the DSC measurement for the solidification range differ by about 15°C (figure 8), these two techniques result in a similar estimate for the effect of 1% Nb on the change in solidification range, i.e., between 67 and 69°C / 1% Nb.

The solidus and liquidus temperatures of the Thermo-Calc modelling and DSC experiment was compared in table 4. The liquidus temperatures for the Thermo-Calc modelling and the DSC experiment were almost the same except the unstabilized alloys A:0Ti;0Nb and B:0Ti;0Nb which were not determined in the DSC experiment. There were minor differences in the solidus temperatures except the G:0.1Ti;0.4Nb and I:0.1Ti;0.5Nb;2Mo alloys which had almost the same values.

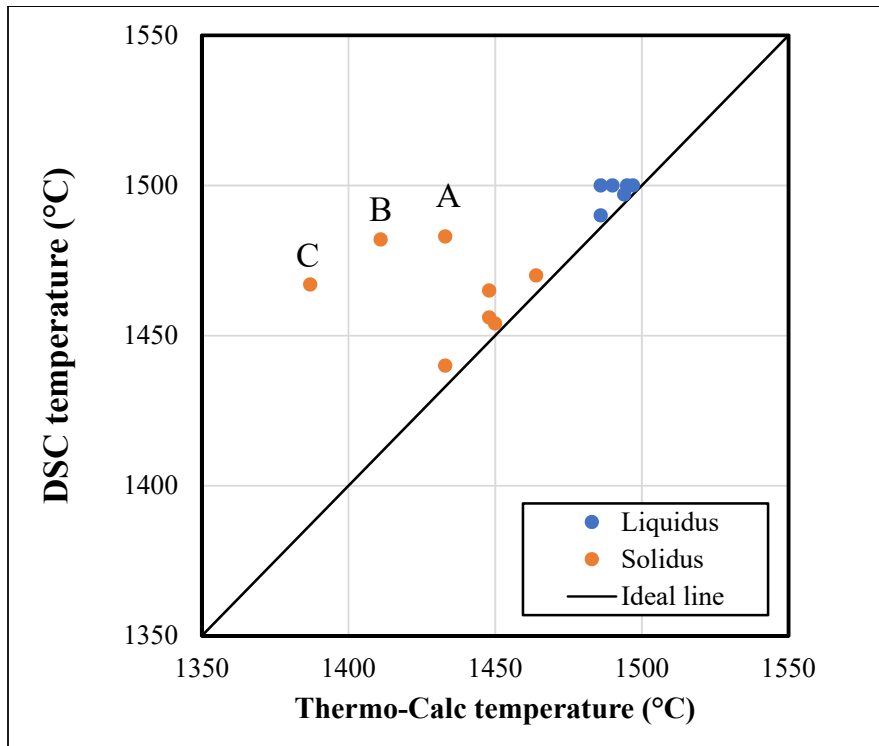


Figure 8. The relationship between DSC measurement (on cooling) and Thermo-Calc for the solidus and liquidus temperature values.

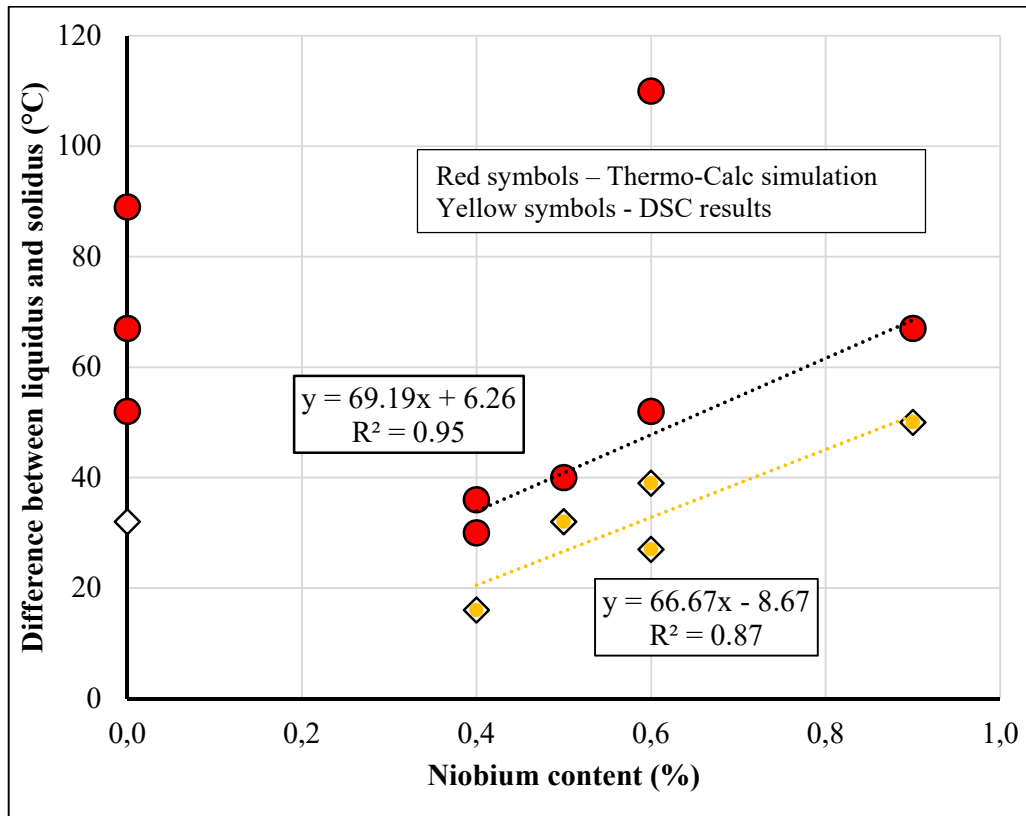


Figure 9. The difference between liquidus and solidus of DSC and Thermo-Calc against Nb content.

Table 4. Comparison of the solidus and liquidus temperatures of the Thermo-Calc modelling and DSC experiment

Sample ID	Thermo-Calc modelling		DSC experiment	
	Liquidus temperature (°C)	Solidus temperature (°C)	Liquidus temperature (°C)	Solidus temperature (°C)
A:0Ti;0Nb	1500	1433	--	1483
B:0Ti;0Nb	1500	1411	--	1482
C:0.7Ti	1497	1387	1497	1465
D:0.6Nb	1500	1448	1494	1467
E:0.4Ti;0.6Nb	1500	1433	1495	1456
F:0.4Ti;0.9Nb	1500	1470	1490	1440
G:0.1Ti;0.4Nb	1500	1464	1486	1470
H:0.1Ti;0.4Nb	1500	1464	N/A	N/A
I:0.1Ti;0.5Nb;2Mo	1490	1450	1486	1454

*N/A = not available

The brittle temperature range (BTR), which is approximated by the difference between the liquidus and solidus temperatures of the material (the solidification temperature range) can be used to explain some observations [3, 19]. The solidification temperature range as estimated using Thermo-Calc seems to reveal the contribution to susceptibility to solidification cracking of these steels. From table 2, showing the Thermo-Calc results, the D:0.6Nb showed the highest difference between the liquidus and solidus value and table 3, with the DSC results, revealed the F:0.4Ti;0.9Nb as having the highest solidification temperature range. The addition of Nb increased the solidification temperature range significantly and thus the alloy containing Nb should be susceptible to solidification cracking [17]. The same authors [17] also stated that Nb contributed more than Ti in the solidification temperature range for the ferritic stainless steels [17]. It was found that the addition of Nb in ferritic stainless steels increased the difference between the liquidus and the solidus temperature and this increased the susceptibility to solidification cracking of the ferritic stainless steel [23].

5. Conclusions

- The Thermo-Calc simulations revealed the various precipitates that occurred during solidification of the ferritic stainless steels.
- The DSC experiment revealed only the formation of δ -ferrite without showing any indication for the onset of precipitates.
- There was some discrepancy between the measured solidification temperature range (using DSC) and the solidification temperature range, as calculated using Thermo-Calc.

Acknowledgements

The authors want to thank Office of Research, Innovation, and Development (ORID), University of Ghana, Department of Research and Innovation Support (DRIS), University of Pretoria and the Southern African Institute of Welding (SAIW) for financial assistance. The

authors are also grateful to Professor Robert Knutsen of the Centre for Materials Engineering at the University of Cape Town, for execution of the DSC experiment.

References

- [1] Lippold J C and Kotecki D J 2005 *Welding Metallurgy and Weldability of Stainless Steels*, 1st ed. New Jersey: John Wiley and Sons, pp. 87-135.
- [2] Krysiak K F, Grubb J F, Pollard B and Campbell R D 1993 Selection of Wrought Ferritic Stainless Steels, in *ASM Handbook, Volume 6: Welding, Brazing, and Soldering*, pp. 443–455.
- [3] Kou S 2003 *Welding Metallurgy*, 2nd ed. New Jersey: John Wiley & Sons, pp. 263-295.
- [4] Lippold J C 2015 *Welding Metallurgy and Weldability*, 1st ed. Hoboken, New Jersey: John Wiley & Sons, pp. 271-278.
- [5] Folkhard E 1988 *Welding Metallurgy of Stainless Steels*, 1st ed. Vienna: Springer Vienna, pp 31-112.
- [6] Gordon W and van Bennekom A 1996 Review of stabilisation of ferritic stainless steels *Mater. Sci. Technol.*, vol. 12, pp. 126–131.
- [7] Fujita N O, Kikuchi K, Suzuki T, Funaki S and Hiroshige L 1996 Effect of Niobium on High Temperature Properties for ferritic Stainless Steel *Scr. Mater.*, vol. 35, pp. 705–710.
- [8] Fujita N, Ohmura K and Yamamoto A 2003 Changes of microstructures and high temperature properties during high temperature service of niobium added ferritic stainless steels *Mater. Sci. Eng. A*, vol. 351, no. 1–2, pp. 272–281.

- [9] Sim G M, Ahn J C, Hong S C, Lee K J and Lee K S 2005 Effect of Nb precipitate coarsening on the high temperature strength in Nb containing ferritic stainless steels *Mater. Sci. Eng. A*, vol. 396, no. 1–2, pp. 159–165.
- [10] Smallman R E and Bishop R J 2002 *Modern Physical Metallurgy and Materials Engineering*, 6th Editio. New York: Butterworth-Heinemann, 2002.
- [11] Yang L 2008 *Materials Characterisation - Introduction to Microscope and Spectroscopy*. Singapore: John Wiley & Sons (Asia) Pte Ltd.
- [12] Konadu D S, Pistorius P G H and Toit M 2019 The influence of Ti and Nb on solidification cracking of ferritic stainless steels, as determined using self-restrained samples *Weld. world*, vol. 63, no. 5, pp. 1163–1172.
- [13] Konadu D S, Pistorius P G H, Toit M D U and Griesche A 2019 Solidification cracking susceptibility of ferritic stainless steels using Modified Vareststraint Transvareststraint (MVT) method *Sadhana*, vol. 44, no. 149, pp. 1–6.
- [14] Cross C E 2005 On the Origin of Weld Solidification Cracking in *Hot Cracking Phenomena in Welds*, Berlin Heidelberg: Springer Berlin Heidelberg, pp. 3–18.
- [15] Ganesh *et al.* B J 2011 Differential Scanning Calorimetry Study of Diffusional and Martensitic Phase Transformations in Some 9 wt- % Cr Low Carbon Ferritic Steels,” *Mater. Sci. Technol.*, vol. 27, no. 2, pp. 500–512.
- [16] Steiner Petrovič D, Klančnik G, Pirnat M and Medved J 2011 Differential scanning calorimetry study of the solidification sequence of austenitic stainless steel,” *J. Therm. Anal. Calorim.*, vol. 105, no. 1, pp. 251–257.
- [17] Shan Y, Luo X, Hu X and Liu S 2011 Mechanisms of Solidification Structure Improvement of Ultra Pure 17 wt % Cr Ferritic Stainless Steel by Ti , Nb Addition *J.*

- Mater. Sci. Technol.*, vol. 27, no. 4, pp. 352–358.
- [18] Park J H 2011 Effect of inclusions on the solidification structures of ferritic stainless steel: Computational and experimental study of inclusion evolution *Calphad*, vol. 35, no. 4, pp. 455–462.
- [19] Notis R M, Gjostein N A, Jessen Jr. N C and Kendall E C 1992 *ASM handbook volume 3 alloys phase diagrams*. ASM International, pp. 841-869.
- [20] Lo K H, Shek C H and Lai J K L 2009 Recent developments in stainless steels *Mater. Sci. Eng. R Reports*, vol. 65, no. 4–6, pp. 39–104.
- [21] Tripathy H, Raju S, Kumar A, Panneerselvam G and Jayakumar T 2013 Thermal stability and thermal property characterisation of Fe–14.4Cr–15.4Ni–2.4Mo–2.36Mn–0.25Ti–1.02Si–0.042C–0.04P–0.005B (mass%) austenitic stainless steel (Alloy D9I) *Nucl. Eng. Des.*, vol. 255, pp. 86–96.
- [22] Martinik *et al.* O 2017 Prediction and Measurement of selected Phase Transformation Temperatures of Steels *J. Min. Metall. Sect. B Metall.*, vol. 53, no. 3, pp. 391–398.
- [23] Konadu D S 2019 The effect of stabilizing elements, specifically titanium and niobium, on the susceptibility of ferritic stainless steels to solidification cracking University of Pretoria, Pretoria, South Africa pp. 171-172.